

Measurements of Micro-Turbulence in High Beta and High Density Regimes of LHD and Comparison with Resistive G-Mode Scaling

Clive MICHAEL, Kenji TANAKA, Leonid VYACHESLAVOV¹, Andrei SANIN¹,
Tsuyoshi AKIYAMA, Yoshiro NARUSHIMA, Kiyomasa WATANABE, Hisamichi FUNABA,
Sadayoshi MURAKAMI², Katsumi IDA, Mikiro YOSHINUMA, Ryuichi SAKAMOTO,
Kazuo KAWAHATA and Shigeki OKAJIMA³

National Institute of Fusion Science, Toki 509-5292, Japan

¹ *Budker Institute for Nuclear Physics, Novosibirsk, Russia*

² *Department of Nuclear Engineering, Kyoto University, Kyoto 606-8501, Japan*

³ *Chubu University, Kasugai 487-8501, Japan*

(Received 7 December 2007 / Accepted 11 March 2008)

Density fluctuations are analyzed in high volume average beta and high core density discharges in the Large Helical Device (LHD) using a 2D phase contrast imaging system and far infra-red interferometer. Both these regimes share similarly high beta gradients and evidence of pressure driven MHD modes is presented. In high volume average beta plasmas, both large and ion-gyro scale density fluctuation levels increase with beta and, in the edge, compare favorably with growth rate of resistive interchange modes, showing additional dependence on density at fixed β . In high core density plasmas with internal diffusion barrier, intermittent fluctuation bursts around mid radius are observed which are triggered when the normalized density gradient exceeds a certain threshold. The intermittent character is stronger for outward shifted plasmas and there appears to be a fluctuation suppression mechanism, possibly related to temperature gradient.

© 2008 The Japan Society of Plasma Science and Nuclear Fusion Research

Keywords: high beta, density fluctuation, phase contrast imaging, MHD, resistive interchange, super dense core regime, ion temperature gradient turbulence

DOI: 10.1585/pfr.3.S1071

1. Introduction

The Large Helical Device (LHD) has set many impressive records with respect to high performance plasma operation, including operation at low field ($B \sim 0.425$ T), high volume average beta (up to 5%) [1], as well as at high field ($B > 2$ T), high central beta with high central density produced through an internal diffusion barrier (IDB) [2]. Since both of these regimes share high pressure (beta) gradients, MHD instabilities such as interchange and ballooning modes may be important for their confinement. Large scale MHD instabilities have been measured with magnetic probes [3, 4]; however, small scale structures may also be excited. While the growth of large scale MHD instabilities can cause rapid reduction of pressure, anomalous transport driven by ion gyro-scale structures may produce a soft limit the attainable plasma pressure.

The 2D CO₂ laser phase contrast imaging system is introduced in Sec. 2. This can measure ion gyro-scale fluctuations with wavenumber $1 < k < 10 \text{ cm}^{-1}$, with moderate spatial resolution from the core to the edge, depending on magnetic configuration. In Sec. 3, turbulence properties measured using this diagnostic are compared to theoretical expectations for resistive interchange modes, calculated on

the basis of profiles from FIR and CO₂ interferometers, and the YAG Thomson scattering system, across a range of discharges at low field, high volume average beta. This complements a study of similar analysis of thermal conductivity [5]. In Sec. 4, we present the dynamical evolution of core turbulence level in dense core discharges for plasmas in configurations with vacuum magnetic axis position $R_{ax} = 3.65$ m, 3.75 m. As these plasmas are non-stationary, a strong intermittency of fluctuation signals is observed. These bursts are correlated with profile relaxations indicating that they are harmful for confinement. In outward configurations which have a more pronounced diffusion barrier, the intermittency is greater suggesting there is another mechanism suppressing these modes. However, the fluctuation level around the foot of the diffusion barrier in between bursts does not appear to be greatly different between these two configurations.

2. Density Fluctuation Measurements with CO₂ Laser Phase Contrast Imaging and FIR Interferometer

For density fluctuation measurements we use the CO₂ laser 2D phase contrast imaging diagnostic for diagnosis of ion gyro-scale fluctuations (with $1 < k < 10 \text{ cm}^{-1}$), and the FIR interferometer [6] for diagnostic large scale

author's e-mail: Clive.Michael@ukaea.org.uk

fluctuations (with $k < 1 \text{ cm}^{-1}$). Phase counters of the FIR have sufficient precision (1/60 fringe) and bandwidth ($f < 50 \text{ kHz}$) to diagnose fluctuations at high beta, though at low beta, the fluctuation level is comparable to the noise. Note that the PCI diagnostic does not admit $k = 0$ components because of its optical arrangement, while the FIR interferometer does. Both the PCI and FIR systems only directly measure the line integrated density fluctuation amplitude, rather than the local value. However, with the 2D PCI diagnostic, some moderate spatial resolution is possible as described below. Routinely the fluctuation components near the edge are much stronger than any core components, so for diagnosis of edge resistive g modes, line-integral values are sufficient, but for detailed analysis, and for analysis of turbulence near the core of high core density discharges, a proper analysis to resolve fluctuations along the line of sight is necessary to analyze changes in core fluctuations as distinct from edge fluctuations.

The 2D phase contrast imaging diagnostic system on LHD employs a 2D imaging principle to split the line-integrated fluctuation signal into contributions from different layers along the line of sight, according to the “magnetic shear” principle [7–9]. The sightline is vertical passing at $R = 3.603 \text{ m}$, so penetrates from the edge to the core, depending on the magnetic axis position of the plasma (R_{ax}), implying core and edge fluctuation components (from both top and bottom) can be separated. The system cannot, however, fundamentally recover the local fluctuation amplitude because of line-integration effects unless the spectrum is isotropic, which it generally is not [10]. Given that the local density is n , and the line-integrated density is $N = \int n dz$ (where the z coordinate is along the probing beam), and fluctuations are denoted with a $\tilde{\cdot}$, $\langle \tilde{N}^2 \rangle$, which is proportional to the variance of the raw signal measured by PCI (over a time window defining the ensemble averaging), can be split up into contributions along the line of sight parameterized by flux coordinate ρ , $n_{\text{fluc}}^2(\rho)$ according to the magnetic shear technique. Though this has been resolved along the line of sight, it still represents a line integral over a distance characteristic of the correlation length. This can be related to the local fluctuation power ($\langle \tilde{n}^2 \rangle$) according to [11]:

$$n_{\text{fluc}}^2(\rho) = \langle \tilde{n}^2(\rho) \rangle l_z l_{\text{res}} \quad (1)$$

where l_z , related to the correlation length, represents the ratio of the fluctuation spectral power density propagating exactly perpendicular to the probing beam to the total fluctuation power, and l_{res} is an instrumental resolution which increases with measured fluctuation wavelength. For typical measurements, the peak wavelength is such that the instrumental width is around half a radius, or less near the edge because the average wavelength is generally smaller than in the core. In the analysis here, no attempt is made to account for l_{res} or l_z . Therefore, note the difference in notation when talking about PCI measured values (n_{fluc}) and true local values (\tilde{n}).

3. High Volume Average Beta

For high volume average beta plasmas, turbulent transport induced by resistive interchange modes, driven by beta gradient in the magnetic hill region in the edge is expected to be a limiting mechanism on the attainable plasma beta in helical devices. In LHD, these modes have been shown to have a “soft” character since their occurrence does not produce a catastrophic effect on plasma operation and since plasma operation has been extended well beyond the Mercier instability boundaries [12]. This is in contrast to pressure (beta) driven instabilities in the edge of Tokamak devices, such as ELMS, which grow very quickly beyond the instability threshold producing a sudden crash, though the physical mechanism may be different, since the Tokamak does not have magnetic hill because the toroidal current is internal to the plasma. Resistive g modes with low order mode numbers are identified with magnetic probes and have been compared successfully to predictions of resistive interchange modes [3, 13], specifically, they have the correct dependence on β and magnetic Reynolds number S (defined after Eq. (2)). However, theoretically, resistive interchange can be excited up to high order mode numbers, up to the dissipative gyro-scale, which can produce an anomalous flux limiting performance since the growth rate increases with β . Previous work on LHD [5] has looked at the role of resistive interchange turbulence and its relationship to the electron heat transport coefficient, and it was shown that at high beta, transport increases more strongly with beta than predicted by a simple gyro-Bohm type model (incorporating drift wave instabilities); and that a model describing resistive interchange turbulence accurately reproduced the beta tendency of electron heat conductivity. This established (1) the role of high beta/resistive g on energy transport. Here, however, we plan to show the other possible links, (2) role of high beta on fluctuations and (3) role of fluctuations on energy transport. This is the first such work of a comparison of density fluctuations and energy transport; previously particle transport coefficients were compared with the fluctuation level in low beta high field discharges [14].

Different “modes” or types of turbulence may have different driving forces, or dependencies on plasma parameters. In such cases, it makes sense to compare fluctuation levels with the expected growth rates; however, one has to bear in mind that the amplitude of the mix of many possible modes may not fit to one single scaling law, this will cause some scatter. A positive correlation between theory and experiment is a positive indication of the applicability of that theory.

Possible modes which could be excited in high beta plasmas include, in addition to resistive interchange modes, current-diffusive ballooning modes [15], which are also driven by beta gradients and may not be so easily distinguished from resistive interchange modes, as well as drift-type instabilities, such as ion temperature gradi-

ent (ITG) and trapped electron modes (TEM). The drive mechanism of these modes do not depend so directly on beta, rather on functions of normalized density (L_n^{-1}) and temperature (L_T^{-1}) gradients such as $\eta = L_T^{-1}/L_n^{-1}$ (although they are known to be stabilized at higher beta [16]).

The characteristic wavelength of the turbulence also depends on its physical origin. MHD type interchange or ballooning instabilities can exist at both macro or micro scales. On the other hand, drift wave turbulence only can exist at the ion gyro-scale. This motivates the comparison of the beta dependence of large and small scale structures as presented below. However, here, we do not look into the details of the macro-modes, or even the relationship between micro and macro-modes (which may be due to Zonal flows or due to the growth rate of modes at both scales having similar beta gradient dependence). Such issues are a topic for future work.

3.1 Theory of resistive interchange and ballooning turbulence

Since resistive interchange and current-diffusive ballooning mode (CDBM) turbulence, are both MHD instabilities driven at high beta, analytic expressions for their growth rates compared. However, it should be noted that the expectation is that resistive g mode turbulence is important at the edge and at high beta, because (1) it is driven unstable by the magnetic hill, and (2) current diffusive ballooning modes are considered as important only at higher temperatures, which occur towards the core.

For resistive interchange modes, an analytic theory, verified by numerical simulation was developed [17–20]. The growth rate is given as:

$$\gamma_{\text{gmod}} = S^{-1/3} \left(\nabla \beta \frac{R_0^2 \kappa_n}{2} m \frac{2\pi q}{s} \right)^{2/3} \tau_{\text{hp}}^{-1} \quad (2)$$

where, m is the poloidal mode number, R_0, a is the major/minor radius, the magnetic Reynolds number $S = \tau_R/\tau_{\text{hp}}$, the resistive skin time $\tau_R = r^2 \mu_0/\eta$, and the poloidal Alfvén time $\tau_{\text{hp}} = R_0 \sqrt{\mu_0 m_i n}/B$, with $\eta \propto T^{3/2}$ being the Spitzer resistivity, R_0 is the major radius, q and s being the safety factor and normalized shear. The term κ_n involves the magnetic curvature, and is positive in regions of magnetic hill. Therefore, the scaling of the growth rate is not simply given by $\beta \propto n_e T_e/B^2$, it is given by:

$$\gamma_{\text{gmod}} \propto n_e^{1/6} (n_e T_e)^{1/6} B^{-2/3} \kappa_n^{2/3} L_p^{-2/3} \quad (3)$$

where $L_p^{-1} = \nabla(n_e T_e)/(n_e T_e)$. On the other hand, the growth rate for the CDBM is [15]:

$$\gamma_{\text{CDBM}} = \hat{\lambda}^{0.2} (mq^2)^{0.8} (q \nabla \beta R_0/a)^{0.6} s^{-0.4} \tau_{\text{hp}}^{-1} \quad (4)$$

where, $\hat{\lambda}$ is related to the current diffusivity. The dependence on plasma parameters and magnetic field strength, (neglecting parameters of the shape of the field) therefore

has the scaling:

$$\gamma_{\text{CDBM}} \propto n_e^{0.1} T_e^{0.6} B^{-0.2} L_p^{-0.6} \quad (5)$$

where the dependence of the term $\hat{\lambda}^{0.2}$ has been neglected since exponent is much weaker than other terms in Eq. (4).

Comparing Eq. (4) with Eq. (2), it is clear that the largest difference between the scaling of these modes with n, T, B is in the resistivity dependence $S^{-1/3}$. Therefore the CDBM and resistive g-mode scaling do not fit the same scaling law and are in principle distinguishable.

According to the simplest form of mixing length theory, the fluctuation level is independent of the growth rate γ :

$$\frac{\tilde{n}}{n} = \frac{1}{k} \frac{\nabla n}{n}. \quad (6)$$

On the other hand, more complete strong turbulence theory states that the diffusivity D (not distinguishing particle or heat) of a simple test mode is given by the diffusivity of the whole turbulent structure, and provides a damping rate $\gamma_{\text{damp}} \sim Dk^2$. Assuming that the growth rate in a nonlinear saturated state is the same as for zero fluctuation level, equating γ with γ_{damp} gives:

$$D = \chi = \gamma/k^2. \quad (7)$$

Under this ansatz, the turbulent flux $D \nabla n$ must be equivalent to $\langle \tilde{n} \tilde{v} \rangle$. Invoking the Boltzman relation $\tilde{n}/n = \tilde{\phi}/T$ with $\tilde{v} = k \tilde{\phi}/B$, one can derive the relation:

$$\left(\frac{\tilde{n}}{n} \right)^2 = \frac{B}{Tk^3} \gamma \left(\frac{\nabla n}{n} \right), \quad (8)$$

which implies that the fluctuation level is indeed governed by the linear growth rate. There criticisms to the use of the “strong turbulence ansatz” above, necessitating the full inclusion of processes such as zonal flows and complete nonlinear mode coupling for calculation of fluctuation levels. However, in many regimes, the effects of zonal flows do not change the zero order scaling of the turbulence, just provide some improvement factor. This has been confirmed in one study [21] in which linear growth rates were shown to faithfully reproduce the non-linear saturation level.

3.2 Fluctuation measurements and consistency with resistive g

For this study, density, temperature and magnetic field strength were systematically varied in a series of discharges in the magnetic configuration with magnetic axis $R_{\text{ax}} = 3.6$ m, helical pitch parameter $\gamma = 1.25$. At certain times during the flat-top of each discharge when the plasma was at equilibrium, fluctuation and parameter profiles were stored in a small database to be analyzed. The range of central densities and electron temperatures, and magnetic field strengths spanned are shown in Fig. (1), together with

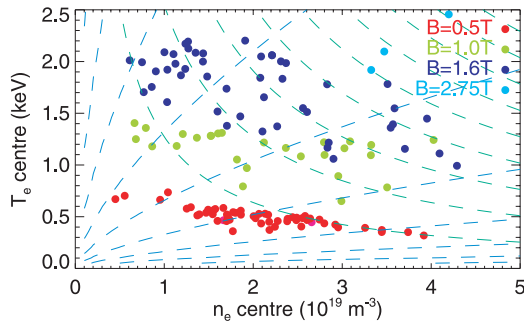


Fig. 1 Density, temperature and magnetic field strengths covered over in the parameter scans, together with contours of β and collision frequency.

lines of constant β , ν_{ei} (related to magnetic Reynolds number S), and gyro-radius. It can be seen that the temperature does not change strongly with density. The volume average β_{vol} reached only up to 3% in these discharges as the helical pitch configuration parameter was $\gamma = 1.25$ rather than $\gamma \sim 1.20$ at which the recent very high beta shots were obtained [1], and since full heating power was not available for scans at $B = 0.5$ T. The value β_{vol} was calculated from measured density and electron temperature values, applying a single correction factor for all discharges to match the average diamagnetic β (this assumes constant Z_{eff}).

The β_{vol} dependence of the raw line integrated fluctuation levels \tilde{N}/N from the FIR and PCI systems as described in Sec. (2) are plotted in Fig. (2). It is clear that for both systems, there is a distinct increasing trend of fluctuation level with β . The increase with β_{vol} appears to be most significant for $\beta_{vol} > 1\%$, consistent with the findings that $\chi_{exp}/\chi_{gmod} = 1$ for $\beta_{vol} > 1\%$ in [5], where χ_{exp} is the experimentally derived thermal conductivity and χ_{gmod} is the resistive g mode conductivity as in Eq. (7). For the 2D PCI (with $k > 1 \text{ cm}^{-1}$), the fluctuation level appears to double roughly as beta goes from $\sim 0.3\%$ to 3%, while for the FIR, which measures $k < 1 \text{ cm}^{-1}$, the increase is much larger. This may be attributed to the fact that resistive interchange turbulence can drive both large scale and ion gyro-scale fluctuations, and has a strong beta dependence, while the level of electrostatic drift wave turbulence (ITG/TEM), which does not depend so explicitly on beta, is strong at the ion gyro-scale but non-existent at large scales. With both diagnostics there also appears to be a large scatter at high β . This is due to (1) the loss of detail due to line-integration effects, and (2) assuming that the resistive interchange mode is responsible for the beta dependence, the growth rate (fluctuation level) should have additional dependence on plasma parameters than simply β_{vol} . This motivates us to examine the local fluctuation level (rather than line integrated), and compare the result with γ_{gmod} formula as written in Eq. (3).

The 2D PCI signals are analyzed according to the technique described in [9, 22] to determine the spatial

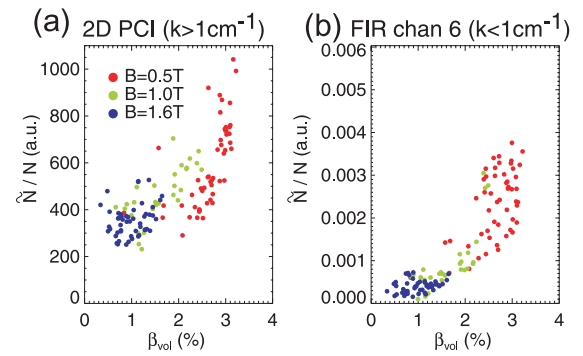


Fig. 2 β_{vol} dependence of line integrated fluctuation level for both (a) ion gyro scale structures with $k > 1 \text{ cm}^{-1}$ from 2D PCI, and (b) large scale structures with $k < 1 \text{ cm}^{-1}$ from the FIR interferometer.

location of the fluctuations along the line of sight. In its simplest form, this generates the fluctuation spectral density per unit k $\partial n_{fluc}^2(\rho, k)/\partial k$ and its integrals $\int \partial n_{fluc}^2(\rho, k)/\partial k dk$, $\int \partial n_{fluc}^2(\rho, k)/\partial k dz$ (where z is the distance along the line of sight). This is plotted for one higher beta discharge in Fig. (3). For this analysis it is necessary to map the sight line geometry to flux coordinates with the appropriate equilibrium. Since the Shafranov shift is non negligible, a different equilibrium set of surfaces is chosen from a VMEC database for each discharge such that the asymmetric part of the electron temperature profile, measured from Thomson scattering, is minimized. In this figure only, the sign of ρ denotes which side of the mid-plane is measured, with positive being above and negative being below. The sign of k indicates the direction of propagation relative to the beam, and the reversal about the center shows the poloidal propagation towards the edge. The mismatch of the upper and lower profiles may be attributable to either (1) because different directional wave-vector components are measured on the top compared with the bottom [10], or because (2) fluctuation structure is not symmetric on a flux surface, however, since the magnetic field structure is symmetric with respect to the top and bottom measurement locations, this explanation is plausible only outside the last closed flux surface. Therefore, in following analysis, we retain information about above and below the midplane as independent measurements. The direction of propagation reverses from top to bottom consistent with there being a poloidal propagation in the electron diamagnetic direction. In other discharges, significant peaks propagate in the ion diamagnetic direction. In a previous study [14], it was shown that the ion diamagnetic components related more clearly to edge particle transport than electron diamagnetic components. However, in this set of discharges, both components seem to have a similar tendency with β . For this reason, and since there is no clear physical interpretation of ion/electron diamagnetic components without poloidal $E \times B$ rotation measurements, analysis of these separated components is not carried out.

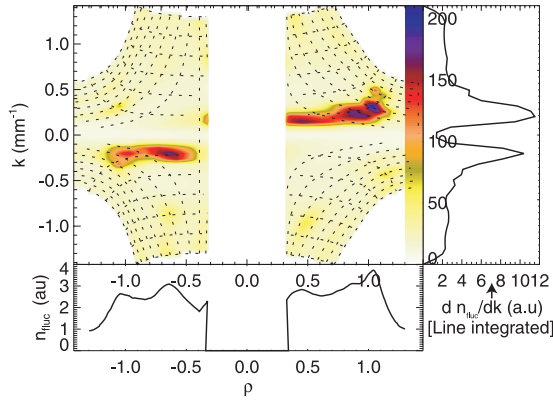


Fig. 3 Analysis of 2D PCI fluctuation images to localize certain fluctuations at particular radii ρ and particular k , for a typical high β shot (#67666@ $t = 3.0$ s). Dashed lines denote the characteristic spatial/ k resolution.

The spatial resolution characterized by the grid in Fig. (3). In the total integral profile $n_{\text{fluc}}(\rho)$, the spatial resolution $\Delta\rho \sim 0.2$ at the edge and around $\Delta\rho = 0.5$ towards $\rho = 0.3$, because the average k is higher towards the edge and since $\Delta\rho \propto 1/k$ [9]. These resolution estimates are conservative; the resolution may be higher due to the Maximum Entropy image processing technique used, which overcomes some of the instrumental resolution degradation [9].

In this shot, two distinct peaks are evident in the profile, around $\rho = 0.5$ and $\rho = 1.0$, as measured from both sides; although, this structure is not universal, in fact many other discharges in this set do not have the peak around $\rho = 0.5$. The relationship of these peaks to plasma density, temperature, pressure gradient and normal curvature κ_n (well/hill) is indicated in Fig. (4). The strongest fluctuation peak appears around $\rho = 1.05$, and appears to correspond roughly to a peak in the pressure gradient profile, plotted in Fig.(4c), demonstrating that pressure gradient may be the free energy source at the edge. However, $\kappa_n > 0$ only outside $\rho = 0.75$ so the fluctuation power inside this radius must be driven by a different mechanism other than resistive interchange, such as ITG/TEM. The presence of the peak outside $\rho = 1$ is suspicious; although not unreasonable considering that the density boundary extends out to about $\rho = 1.15$ according to interferometer measurements. MHD instabilities are not well described theoretically in regions where there are no closed flux surfaces, so it is difficult to judge whether this contradicts or is consistent with the expectations of resistive interchange turbulence. There may also be small systematic position identification error of a few percent.

Taking the component at $\rho = 0.9$, we compare the local n_{fluc}/n with γ_{gmod} from Eq.(3) in Fig. (5). This incorporates the scaling with L_p , n , T , B as well as κ_c which depends on β . It can be seen that there is a much clearer relationship than in Fig. (2), particularly at higher γ . The

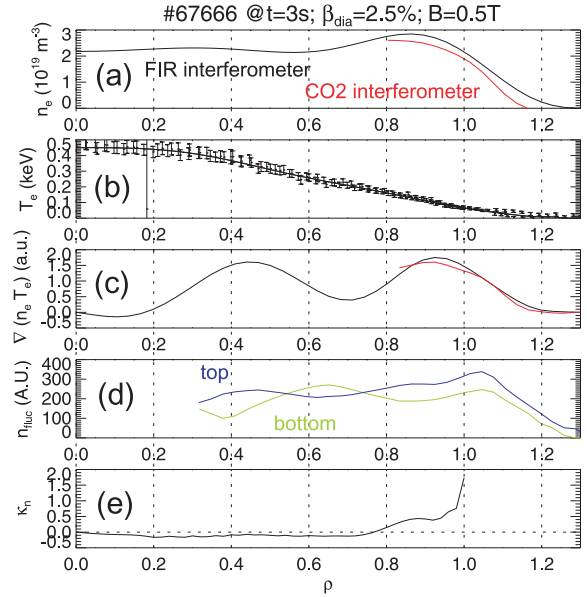


Fig. 4 Comparison of profiles (a) density, (b) temperature, (c) pressure gradient, (d) fluctuation amplitude, and (e) normal curvature κ_n for a shot with $\beta_{\text{vol}} = 2.5\%$.

cause of this better agreement is the increased density dependence arising from the S dependence in Eq. (2), as well as the locality of the measurement; components from the core do not contribute to the plotted signal. While some spatial averaging, characteristic of the PCI radial resolution $\Delta\rho$, should be performed over $n_e(\rho)$, $T_e(\rho)$, and $\kappa_n(\rho)$, there is a strong change in $\kappa_n(\rho)$ between 0.8 and 1.0 which produces an undesired stronger weighting towards $\rho = 1.0$ where uncertainties are greatest. Therefore, no extra spatial averaging is performed for this figure. On the other hand, at positions closer to the core, n_{fluc}/n is not so clearly correlated with the local γ_{gmod} . There still exists a degree of scatter within the data, but within the confidence interval of the trendline (indicated by dashed lines), the trend is at worst flat. (One source of scatter may be due to variation of the correlation length parameter l_z shown in Eq. (1). This would arise if k_r, k_θ spectrum was changing according to other indirect phenomena, such as change of $E \times B$ or magnetic shear.) The points with higher n_{fluc}/n and higher γ_{gmod} , which are essential for observing an increasing tendency, occur at higher β . This suggests that at lower β , the signature of resistive g modes may not be so clear compared to other types of turbulence. It was also observed in [5] that, for $\beta < 1\%$, χ was more consistent with that given by a gyro-bohm model (controlled by ITG turbulence) than at higher β .

This agreement is evidence that the underlying turbulence may be controlled by resistive g modes, but does not equivocally prove it. To consider the current diffusive ballooning mode as another possible candidate, the fluctuation level was also compared with γ_{CDBM} as in Eq.(5). It was found, however, that n_{fluc}/n decreased with γ_{CDBM} be-

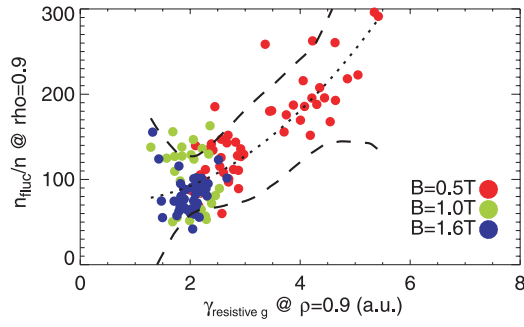


Fig. 5 Comparison of local fluctuation amplitude n_{fluc}/n at $\rho = 0.9$ and resistive g driving growth rate γ_g at the same ρ . Dotted line indicates a best fit parabolic trend-line (with a total square residual χ_0^2), and dashed lines indicate the confidence interval, such that $\chi^2 = 2\chi_0^2$.

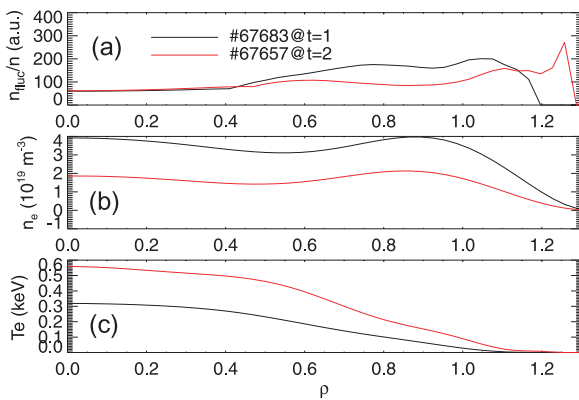


Fig. 6 For shots with similar β_{vol} , but significantly different density, comparison of profiles of (a) fluctuation level n_{fluc}/n , (b) density, (c) temperature.

cause the temperature dependence is much stronger than density or magnetic field dependence, so that at higher β , where n_{fluc}/n is larger, and the temperature is lower, γ_{CDBM} is smaller. Such an inverse correlation is unlikely so that we can probably dismiss the CDBM as a candidate mode.

The increased density dependence with respect to temperature, which is evidence of the dependence on $S^{-1/3}$, or resistivity, is highlighted by comparing 2 discharges with similar β_{vol} , but significantly different density. The profiles of fluctuation level n_{fluc}/n , n , T and are compared in Fig. (6). It is clear that the higher density discharge has about twice the fluctuation level, and is largest between $\rho = 0.8 - 1.0$ where resistive g is located. The scaling of fluctuation level here is clearly attributable to stronger density, despite having similar β_{vol} . In Fig. (6a), the relative fluctuation level is not reliable in the region where density is close to zero because of the finite spatial resolution.

The position of the strongest fluctuation peak as a function of β_{vol} is plotted in Fig. (7), separated out into parts above and below the mid-plane, as discussed before. The difference in the character of the upper side compared

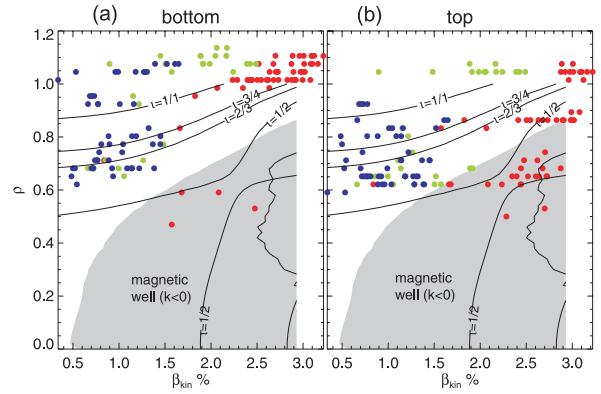


Fig. 7 Position ρ of strongest peak of $n_{\text{fluc}}(\rho)$ on (a) bottom and (b) top sides of the midplane, as a function of β_{vol} , compared with changes in the magnetic structure including well/hill boundary and rational surfaces

with the lower side may be an instrumental effect of having different correlation length l_z (as indicated in Eq. (1), due to anisotropy). However, they both seem to exhibit the same tendency, possibly with a slight shift in position, which may also be a systematic error of the instrument due to slight rotation of the probing laser beam. As β_{vol} is increased, the region of magnetic well extends towards the edge, as indicated by the shaded region, meaning that the resistive g peaks must be localized further towards the edge at higher beta. This seems to be consistent with the measured positions, indicated by dots, more particularly for components on the bottom. For components on the top, there appears to be a concentration of peaks around the $\iota = 1/2$ rational surface, approximately where the magnetic shear is close to zero. This type of MHD activity close to rational surfaces has also recently been reported in [23].

Towards the edge (around $\rho = 0.9$), observed fluctuations are consistent with the growth rate of resistive g modes, however, towards the core, the relationship is not so clear. Considering that appreciable fluctuation power exists in regions of magnetic well, according to Fig. (7), it is likely that the resistive g mode turbulence is not so important there.

3.3 Comparison of fluctuation amplitude with power balance χ at high β

The role of fluctuations on confinement itself is very important to confirm the original assertion that transport is dominated by anomalous processes; and to check that the measured fluctuations are important for confinement, even regardless of the role of what is the driving mechanism of the fluctuations (resistive g or drift wave). For the set of discharges analyzed above, power balance analysis was carried out to determine the “effective” thermal conductivity $\chi = (\chi_e + \chi_i)/2$ as per the procedure described in [5], based on the FIT code [24] which computes the

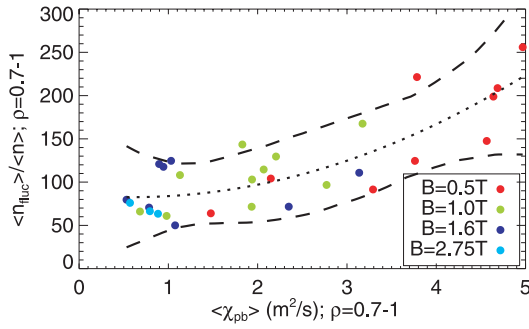


Fig. 8 Comparison of χ with n_{fluc}/n from 2D PCI at $\rho = 0.95$.

power deposition from NBI by calculating fast particle orbits and their interactions with bulk plasma. The PROCTR code [25] is then used to analyze the diffusivity.

We choose to compare the local fluctuation level, averaged over the range $\rho = 0.7 - 1.0$ with the χ averaged over the same interval. This is in order to match the spatial resolution of χ with that of the fluctuation level. The results, for a selected subset of shots in the previous section are plotted in Fig. (8). It is clear that there is an increasing trend of fluctuation level and conductivity. A few data points were placed here for high field discharges ($B = 2.75\text{ T}$). These points illustrate the confinement improvement that occurs with increasing the magnetic field strength. A quadratic curve of best fit and its confidence interval is indicated; they show that there must be an increasing tendency of fluctuation level with χ . The slope of the curve is more shallow at lower χ_{pb} (at higher B), indicating that there may be a more complicated dependence between density fluctuation level and heat transport. In addition, since the temperature gradient may relax to value depending on the input power, n_{fluc}/n was also compared with $q/n = \chi \nabla T_e$, however the scatter was much larger on account of variances in ∇T_e .

Since fluctuation level is connected to χ and it has also been demonstrated that resistive g modes control the fluctuation level in the edge, this supports the idea that edge transport, and hence plasma performance, is effected by resistive g modes at high β . This is consistent with the findings of power balance analysis [5], and as well the S dependence of macro-scale magnetic fluctuations [3].

4. High Core Density

Recently, pellet-fuelled high density plasmas were achieved with central density approaching 10^{21} m^{-3} [2,26]. These plasmas are characterized a high density core with a “diffusion barrier” around mid radius, correlating with the position of zero magnetic shear. Though these plasmas are made at high field ($B > 2\text{ T}$), the central beta approaches that of the high volume average beta plasmas, and so the beta gradients in the diffusion barrier region are very high; therefore they may have some similar characteristics to high volume average beta plasmas. (However, the max-

imum volume average beta is somewhat lower than low field discharges, being around 1.2 - 1.5 % in discharges analyzed here.)

It is suspected that turbulence suppression is responsible for the diffusion barrier. Here the relationship between fluctuation properties around the diffusion barrier, between $\rho = 0.3 - 0.7$, and central pressure, as a measure of energy/particle confinement, shall be analyzed. Also, the fluctuation driving forces including density, temperature and pressure gradients are analyzed in order to understand what factors influence the fluctuation level.

Resistive interchange turbulence may play a role in these discharges. As β_{vol} increases, the region of magnetic hill moves towards the periphery as shown in Fig. (7). Since the magnetic well/hill boundary passes through the region of interest, $0.3 < \rho < 0.7$, and $\beta_{\text{vol}} < 1.5\%$, it is possible for the resistive interchange mode to be destabilized. However, without detailed analysis of the MHD equilibrium, incorporating the measured pressure profile, it is difficult to conclude whether the diffusion barrier is in a location of magnetic hill. On the other hand high pressure gradients may excite other types of MHD instabilities such as current-diffusive ballooning modes [15]. Drift wave like ITG/TEM modes may also be destabilized as discussed in Sec. (3). However, since it is thought that strong $E \times B$ shear may be important for the diffusion barrier formation, changes in the fluctuation level might not relate to changes in the linear growth rate of instabilities, rather to the drive mechanisms for $E \times B$ flow shear.

It has been shown in [26] that the maximum density increases with R_{ax} , and there is a sudden increase between 3.65, and 3.75 m, which is associated with the formation of a steep density gradient or diffusion barrier, as shown by the density profiles in Fig. (9). Fluctuation and profiles are compared between these two configurations in Fig. (10). The central pressure rises after the last pellet injection. It rises faster and to a higher value at $R_{\text{ax}} = 3.75\text{ m}$ compared to $R_{\text{ax}} = 3.65\text{ m}$, as illustrated in Fig. (10a), indicating improved energy confinement.

Because the vertically directed 2D PCI sightline is located at a major radius $R = 3.603\text{ m}$, the system is not sensitive to core fluctuation properties in configurations with strongly outward shifted magnetic axis. In particular, for the highest performance around $R_{\text{ax}} = 3.9\text{ m}$, the mid-radial position cannot be accessed by the present 2D PCI diagnostic. Therefore in this analysis, fluctuation and plasma properties are compared only between $R_{\text{ax}} = 3.65\text{ m}$ and $R_{\text{ax}} = 3.75\text{ m}$. This enables fluctuation properties just at the foot of the diffusion barrier to be compared.

4.1 Analysis of fluctuation properties at $R_{\text{ax}} = 3.65\text{ m}$ and 3.75 m

Fluctuation amplitude is mapped to ρ using a VMEC equilibrium considering the Shafranov shift, dependent on vacuum R_{ax} and β , determined from the CO2 laser interferometer. Since this diagnostic shares the same vertical

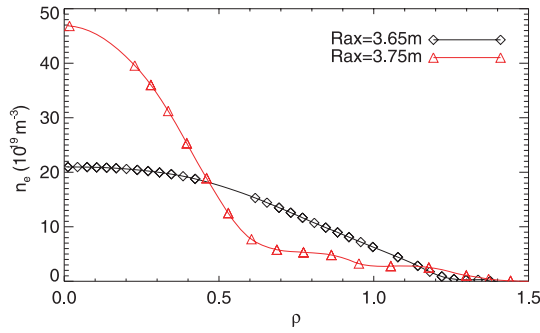


Fig. 9 Comparison of Density profiles between $R_{ax} = 3.65, 3.75$ m (#68956, #68996), at $t - t_0 = 0.2$ s from CO2 laser interferometer. Points denote where lines of sight are tangent to flux surfaces, giving an approximate measure of spatial resolution.

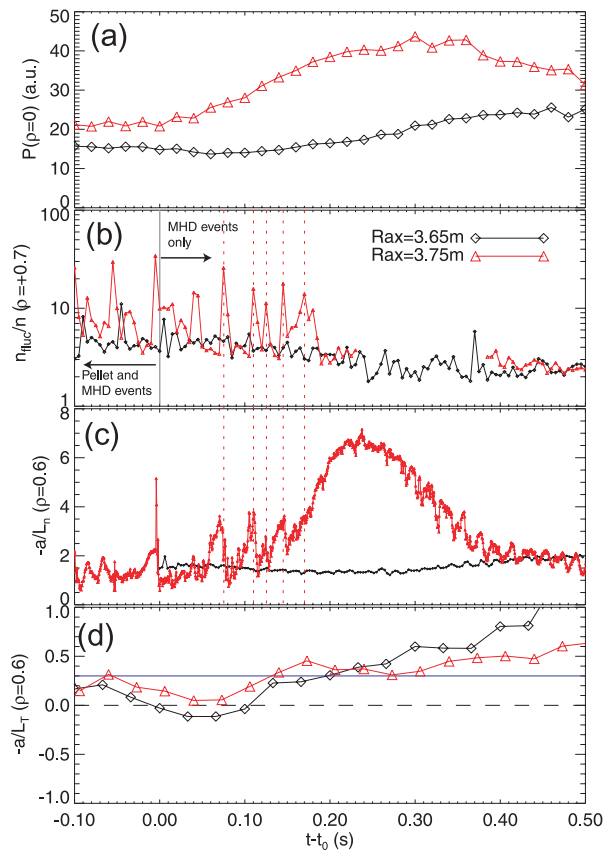


Fig. 10 Comparison between $R_{ax} = 3.65$ m and 3.75 m of (a) Central pressure (from Thomson scattering), (b) Normalized fluctuation level at $\rho = 0.7$, (c) Normalized density gradient, (d) Normalized temperature gradient.

cross-section as 2D PCI, there is very good certainty about the accuracy of the flux surface mapping. The time evolution of fluctuation amplitude (non normalized) $n_{fluc}(\rho)$ is plotted in Fig. (11) for $R_{ax} = 3.65, 3.75$ m. At 3.75 m, the inaccessible region in the core is broader and increases more strongly with time owing to the higher pressure and stronger Shafranov shift.

Because of moderate spatial resolution, it is possible for core fluctuation signals to be influenced by the periphery. For this reason, dots are placed over the each peak, on the upper and lower sides. There is a slight difference between the location of the upper and lower peak which is most likely due to an uncalibrated rotation of the beam by a few degrees; the true fluctuation position should be the average value of the top and bottom measured positions. It can be seen that the peaks are located around $\rho = 0.5/0.6$ at 3.65 m and $\rho = 0.7/0.8$ at 3.75 m.

The time history of the relative fluctuation level, normalized to the density measured from the CO2 laser interferometer, is compared between the two configurations at $\rho = 0.7$ in Fig. (10b). The fluctuation behavior changes strongly in time after pellet injection. For a certain time, temporal bursts in the fluctuation level occur, after which the fluctuation level is dramatically reduced. At $R_{ax} = 3.75$ m, the temporal behavior is much more intermittent, consisting of large short-lived bursts with a certain period in between the bursts. For the moment the fluctuation level between burst events will be compared between $R_{ax} = 3.65, 3.75$ m, to clarify whether the background turbulence plays a role on the formation/existence of the density barrier. Returning to Fig. (10b), the fluctuation level is comparable between the two cases, suggesting little difference of the “non-intermittent” confinement characteristics around $\rho = 0.7$, which is outside, or just at the foot of, the diffusion barrier. (At $\rho = 0.6$, the calculated fluctuation level is lower at $R_{ax} = 3.75$, because the density is much different than $\rho = 0.7$, but we cannot accept this result because this is less than the spatial resolution of PCI). However, this does not discount a change of the fluctuations in the barrier.

The bursting activity has a different effect on confinement. The normalized density gradient $\nabla n/n = L_n^{-1}$, computed from the CO2 laser interferometer [27] is plotted in Fig. (10c), and the normalized temperature gradient, evaluated from a 6th order polynomial fitted to Thomson scattering temperature profile, L_T^{-1} , is plotted in Fig. (10d). There is a clear correlation between the timing of fluctuation burst events at $R_{ax} = 3.75$ m, and crashes in the normalized density gradient, indicating that these modes are responsible for a serious and sudden degradation in confinement. However, the loss of gradient is only observed around $\rho = 0.6$; towards the core, there is no change in density. Moreover, several bursts appear to be triggered at approximately the same threshold in L_n^{-1} , suggesting that these are driven by either density or pressure gradient, since the temperature gradient scale length does not significantly change over the timescale of these events. After $t - t_0 = 0.18$ s, the bursting ceases and the normalized density gradient steepens further without any crash events. This suggest that something has changed to suppress these modes. One possibility is that at this point the $E \times B$ flow shear has increased leading to a suppression of modes [15]. From an extrinsic point of view, the temperature gradient

is increasing in this time, and it may pass a critical value required to suppress the mode. A guess of such a threshold is indicated by the horizontal line in Fig. (10d). (Further towards the core, L_T^{-1} switches sign around the same time as the suppression of burst events, indicating that the global peakedness of the temperature profile is important for this suppression). The strong intermittency of modes suggests there is a force suppressing these at $R_{ax} = 3.75$ m. At $R_{ax} = 3.65$ m, on the other hand, modes still appear to have an intermittent burst like character. Bursts appear to be more frequent and to a lower level. This is clearly evidenced by the non normalized signal plotted in Fig. (11b). Though these modes have a lower level, they persist longer, suggesting that they may be causing a more continuous confinement degradation. Therefore the balance between fluctuations and gradients has a more soft relationship at 3.65 m, and a hard threshold at 3.75 m. The mechanism for this change in the change of character may be critical for the formation the diffusion barrier. Also, the core density collapse event often observed at far outward shifted configurations [28] may be a variant of the smaller collapse events at $R_{ax} = 3.75$ m.

Since the ceasing of the fluctuation bursts may be related to the temperature profile inverting from hollow to peaked, and since the temperature profile is more hollow at $R_{ax} = 3.65$ than 3.75 (indicated by the magnitude of L_T^{-1} in Fig. (11d)), control of the temperature profile by magnetic axis position may be the reason for reduced fluctuations, and hence improved confinement at $R_{ax} = 3.75$ m.

The PCI diagnostic can measure phase velocity, which is related to $E \times B$ rotation; however, towards inner radii, where the sight line is close to tangent to the flux surface, the instrument is not sensitive to the poloidal rotation. In the future, adjusting the system to measure at an outward shifted sightline will allow the poloidal rotation to be measured in the barrier, and allow core fluctuations to be measured to complement this understanding of the physics outside the barrier.

5. Summary

In high volume beta plasmas, the edge fluctuation level increases with local beta gradient and density consistent with a model for resistive g turbulence, but inconsistent with a current-diffusive ballooning mode model. The fluctuation level towards mid radius is unexplainable by resistive g, possibly due to ITG/TEM turbulence. Large scale fluctuations have a much stronger beta dependence than ion gyro-scale fluctuations, probably on account of the ITG/TEM at the ion gyro-scale. Turbulence also is observed around zero shear rational surfaces, suggesting these trigger other MHD activity. For constant beta, lower density, higher temperature is favorable for reduction of the fluctuation level and improvement of confinement. On the other hand, higher density is favorable for increasing the fraction of neutral beam power which is absorbed by

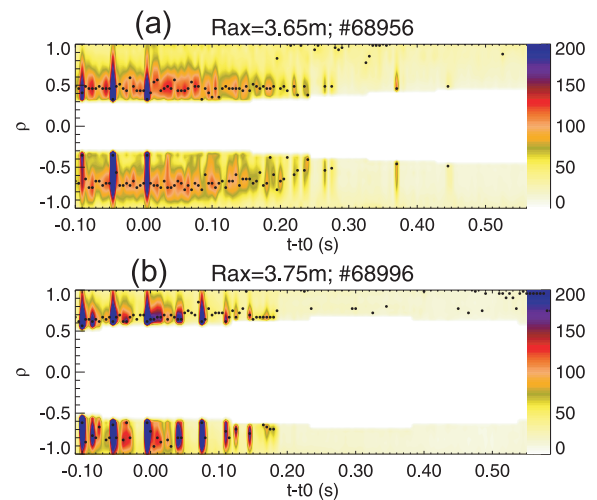


Fig. 11 Spatial temporal map of fluctuation amplitude from 2D PCI, mapped to flux coordinate using appropriate time-dependent Shafranov shift.

the plasma. Therefore, this indicates that appropriate particle control in the edge, for example using the divertor, is necessary to increase the injected power and reduce the thermal conductivity.

At high density, core fluctuations are burst-like character indicating that they are limiting the attainable pressure gradient and a cyclical relaxation similar to ELMS is observed. At inward shifted configurations, without a diffusion barrier, continuous bursts occur suggesting they are continuously limiting the pressure gradient, while at outward shifted configurations, there is a large gap between bursts where the pressure gradient can grow to a much higher value than inward shifted configurations. At some moment, possibly related to the change of the temperature profile from hollow to peaked, the fluctuation bursts cease and the pressure gradient continues further. This suggests another mechanism is controlling the saturation level/stability of these modes, such as $E \times B$ flow shear [20], and that temperature gradient may be a controlling parameter for this mechanism.

Acknowledgments

This work was supported by a grant-in-aid from the Japan Society for the Promotion of Science (JSPS). The authors are thankful to O. Yamagishi of NIFS for advice on the interpretation of growth rates, and to the reviewer for valuable comments. The authors are indebted to the entire LHD experimental group for machine operation.

- [1] K.Y. Watanabe, Confinement study on the reactor relevant high beta LHD plasmas. *these proceedings*, (2008).
- [2] N. Ohya *et al.*, Phys Rev Lett **97**, 055002/1 (2006).
- [3] S. Sakakibara *et al.*, Fusion Sci. Technol. **50**, 177 (2006).
- [4] K.Y. Watababe *et al.*, Nucl. Fusion **45**, 1247 (2005).
- [5] H. Funaba *et al.*, Fusion Sci. Technol. **51**, 129 (2007).

- [6] K. Kawahata *et al.*, Fusion Eng. Des. **34-35**, 393 (1997).
- [7] A.L. Sanin *et al.*, Rev. Sci. Instrum. **75**, 3439 (2004).
- [8] L.N. Vyacheslavov *et al.*, IEEE Trans. Plas. Sci. **33**, 464 (2005).
- [9] C.A. Michael *et al.*, Rev. Sci. Instrum. **77**, 10E923 (2006).
- [10] C.A. Michael *et al.*, Plasma Fusion Res. **2**, S1034 (2007).
- [11] H. Wiesen *et al.*, Plasma Phys. Control. Fusion **30**, 293 (1988).
- [12] K.Y. Watanabe *et al.*, Nucl. Fusion **45**, 1247 (2005).
- [13] A. Komori *et al.*, Phys. Plasmas **12**, 56122 (2005).
- [14] K. Tanaka *et al.*, Fusion Sci. Technol. **51**, 97 (2007).
- [15] K. Itoh *et al.*, Plasma Phys. Control. Fusion **36**, 279 (1993).
- [16] P. Snyder. Phd thesis, Princeton, (1999).
- [17] B.A. Carreras *et al.*, Phys Fluids **30**, 1388 (1987).
- [18] B.A. Carreras and P. H. Diamond, Phys. Fluids B **1**, 1011 (1989).
- [19] M. Wakatani. Resistive interchange turbulence. *AIP Conference Proceedings. Two-Dimensional Turbulence in Plasmas and Fluids. Canberra, ACT, Australia*, page 141 (1997).
- [20] K. Itoh *et al.*, Plasma Phys. Control. Fusion **36**, 123 (1993).
- [21] T. Dannert and F. Jenko, Phys. Plasmas **12**, 72309 (2005).
- [22] C.A. Michael *et al.*, Image analysis method for spatial localization of fluctuations using 2d phase contrast imaging on LHD. *submitted to Rev. Sci. Instrum.*, (2008).
- [23] K. Ida *et al.*, Phys. Rev. Lett. **100**, 045003 (2008).
- [24] S. Murakami *et al.*, Fusion Technol. **27**, 256 (1995).
- [25] H. Howe, ORNL/TM-11521 (1990).
- [26] R. Sakamoto *et al.*, *These proceedings* (2008).
- [27] K. Tanaka *et al.*, Plasma Fusion Res. **2**, S1033 (2007).
- [28] J. Miyazawa *et al.*, *These proceedings*, (2008).